MATERIALS SCIENCE

Biomimetic thermoresponsive superstructures by colloidal soft-and-hard co-assembly

Dengping Lyu[1], Wei Xu[1], Nansen Zhou[2], Wendi Duan[1], Zhisheng Wang[1], Yijiang Mu[1], Renjie Zhou[2], Yufeng Wang[1]*

Soft-and-hard hybrid structures are ubiquitous in biological systems and have inspired the design of man-made mechanical devices, actuators, and robots. The realization of these structures, however, has been challenging at microscale, where material integration and actuation become exceedingly less practical. Here, through simple colloidal assembly, we create microscale superstructures consisting of soft and hard materials, which, serving as microactuators, have thermoresponsive shape-transforming properties. In this case, anisotropic metal-organic framework (MOF) particles as the hard components are integrated with liquid droplets, forming spine-mimicking colloidal chains via valence-limited assembly. The chains, with alternating soft and hard segments, are referred to as MicroSpine and can reversibly change shape, switching between straight and curved states through a thermoresponsive swelling/deswelling mechanism. By solidification of the liquid parts within a chain with prescribed patterns, we design various chain morphologies, such as "colloidal arms," with controlled actuating behaviors. The chains are further used to build colloidal capsules, which encapsulate and release guests by the temperature-programmed actuation.

INTRODUCTION

Many biological organisms, ranging from mammals to arthropods and microorganisms, contain structures of synergistically integrated soft and hard components (*1*–*4*). Adopting unique spatial arrangements and existing at different length scales, these hybrid structures are responsible for the diverse mechanical properties and functions entailed by biological systems. As a typical example, the human spine has alternating stacks of hard bones and soft intervertebral discs, which is an essential architecture that supports human body weight while maintaining body flexibility. Arguably, mimicking the soft-hard structures in nature has inspired the design of intelligent man-made mechanical devices such as actuators and robots (*5*–*9*).

At macroscale, the integration of soft and hard materials is relatively easy to implement. Various devices with combined compositions in proper structures have been manufactured to perform a range of mechanical functions, including loading, gripping, and moving (*6*, *9*–*14*). By contrast, the miniaturization of similar structures and functions, as an effort to make microactuators, is much more challenging (*15*, *16*). At smaller length scales (micrometer and below), both material integration and arrangement as well as their actuation become less practical. Albeit challenging to make, these microactuators are desirable for making microrobotics, which can be potentially used for minimally invasive diagnostics, targeted drug delivery, and localized sensing (*17*–*19*).

Current fabrication of microactuators mainly relies on top-down methods (*20*–*23*), primarily lithography. Although lithography can produce complex patterns, the material scope has been rather limited. It is thus difficult to combine mechanically distinct components, in this case, the soft and hard materials. In addition, these methods require tedious, multistep processes and suffer from a low yield. They usually produce structures larger than hundreds of micrometers, and further miniaturization, down to several and tens of micrometers, is less feasible and even prevented.

In circumventing these challenges, we envision the use of colloidal assembly (*24*–*26*) to build microactuators, in which nano- and microparticles spontaneously organize into ordered spatial patterns. Because particles of various compositions can in principle be used, including metals, polymers, and oxides (*27*–*31*), their intrinsic properties can be used to impart mechanical strength and the responsiveness to external stimuli. As a bottom-up approach, self- and co-assembly should produce microactuators in a high yield with simple steps. However, despite these advantages, colloidal assembly has been used only in a few systems, such as magnetic cube-based microrobots (*32*) and actuating chain of polymer beads (*33*). Assembling soft and hard materials to make biomimetic superstructures and actuators has yet to be demonstrated.

Here, by exploiting colloidal assembly, we introduce a supra-colloidal, spine-mimicking microactuator, MicroSpine, which integrates soft and hard components and has thermoresponsive shape-transforming properties. MicroSpine is co-assembled by rigid metal-organic framework (MOF) particles and shape-changing liquid droplets, arranged at alternating locations and forming colloidal chain architecture. The chains can reversibly actuate by switching between straight and curved conformations as a thermoresponsive swelling agent diffuses in and out of the oil droplets. By solidification of the liquid droplets at specified chain locations using a customized microscope, we design various chain morphologies and precisely tune their actuation behaviors. Furthermore, MicroSpine is used to build capsules, which can encapsulate and release colloidal guests as regulated by temperature.

[1]Department of Chemistry, The University of Hong Kong, Pokfulam Road, Hong Kong SAR, China. [2]Department of Biomedical Engineering, The Chinese University of Hong Kong, Shatin, Hong Kong SAR, China.
*Corresponding author. Email: wanglab@hku.hk

RESULTS

The soft and hard components

The spinal column of human (or animals) features hard vertebrae connected by soft intervertebral discs, with the endplates serving as the interface (Fig. 1A). The vertebrae support the weight of human body and protect the spinal cord, while the intervertebral discs keep the spine flexible and allow different body gestures (*1*, *2*). The spinal discs can also swell or deswell by absorbing or releasing fluid, in response to body pressure change. To make MicroSpine, the microscale counterpart of spine, our strategy is to combine soft and hard materials at the colloidal level and arrange them in alternating locations, all enabled by assembly. Besides, we design a similar swelling/deswelling mechanism to adjust the volume of the soft component, making MicroSpine responsive (Fig. 1B).

The soft component chosen is a thermoresponsive, shape-tunable liquid (Fig. 2A). It is based on an oligomeric organosilane oil, derived from 3-(trimethoxysilyl)propyl methacrylate (TPM) via hydrolysis and oligomerization in aqueous solution (*34*) (see Materials and Methods). TPM oil can adopt different forms, either as colloidal droplets or thin films depending on the conditions of wetting (as we discuss later). When combined with a temperature-sensitive swelling agent, TPM oil changes its volume and shape accounting for the responsiveness and actuation of MicroSpine (Fig. 2B). Using uniform TPM oil droplets as models, below we first demonstrate its thermoresponsive property, which can be directly applied when TPM is later incorporated in MicroSpine.

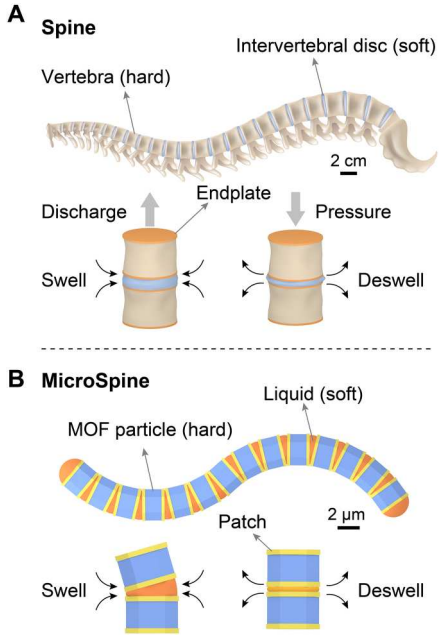

Fig. 1. Structure of spine and MicroSpine. (**A**) Representation of human spine structure, which contains hard vertebrae connected by soft intervertebral discs. The hard and soft components are bridged by the endplates (orange plates) as interface. Also shown is an illustration of the swelling/deswelling property of the intervertebral discs in response to body pressure. (**B**) MicroSpine chain, a microscale actuator that mimics the soft-hard architecture of spine, is assembled by hard MOF particles and soft oligomeric liquid interfaced by the patch structure (yellow plates). Schematics (bottom) show that MicroSpine imitates the working mechanism of spine.

TPM oil droplets 1.1 ± 0.1 μm in diameter are synthesized and mixed with Pluronic L61 (or PL61), the swelling agent (Fig. 2, A to D). PL61 is an amphiphilic triblock copolymer of PEO_2-PPO_{30}-PEO_2 [polyethylene oxide (PEO); polypropylene oxide (PPO)], as shown in Fig. 2C. At low temperatures, the polymer is completely soluble in aqueous conditions [pure water or *N*,*N*′-dimethylformamide (DMF)/water cosolvent]; upon heating, the polymer becomes more hydrophobic and phase separates from solution (fig. S1). The transmittance of a PL61 solution (0.5 wt % in 20% DMF/water) at different temperatures indicates a cloud point temperature of 30.0°C. With TPM droplets present, the insoluble aggregates of PL61 at high temperatures can enter and dissolve in the TPM oil, expanding the size of the droplets (Fig. 2, B and D, and movie S1). Unexpectedly, the diameter of droplet increases linearly over temperature, from 1.3 μm at 20°C to 2.0 μm at 80°C (Fig. 2E and note S1). The size-changing process is fully reversible, whereby the droplets shrink at lower temperatures as PL61 becomes hydrophilic and diffuses out of the TPM oil (Fig. 2F). The droplets remain uniform at all temperatures.

The change in size of the TPM oil droplets also depends on the concentration of PL61, which determines the maximum degree TPM can swell. Figure 2G and fig. S2 show the sizes of the droplets with an increasing PL61 concentration (while the number of droplets is kept constant). For example, when 0.5 wt % of PL61 is included in the system, the expanded droplet at 80°C is around four times the volume of the initial one at 20°C.

In choosing the hard component for MicroSpine, several requirements are to be satisfied. Apart from being mechanically rigid and nondeformable, the material should exist in uniform colloidal sizes. Moreover, it should have favorable interaction with TPM droplets to enable the soft-hard material integration via assembly. Last, the valence of the assembly (i.e., number of colloidal bonds each particle forms) must be well controlled to spontaneously result in the desired linear alternating structure.

For this purpose, we select MOF and, specifically, MIL-96 [Materials Institute Lavoisier (MIL)], a framework of aluminum ions and trimesate ligands (*35*). As a rigid, crystalline framework, MIL-96 can be synthesized as uniform colloidal particles several hundred nanometers to several micrometers in size (*31*, *36*). The particles adopt various polyhedral shapes of the hexagonal crystal family, including short hexagonal cylinders, which we mainly use here (Fig. 3A). Previously, we have shown that the two hexagonal (002) facets (i.e., the top and bottom facets of the hexagonal cylinder) of MIL-96 can be selectively modified by growing a thin layer of zirconium-terephthalate framework, UiO-66 (Universitetet I Oslo) (Fig. 3, A and B, and fig. S3) (*37*). As we discuss below, the UiO-66–modified facets, serving as sticky surface "patches," provide specific interaction that combines the MIL-96 body with the soft component.

Valence-controlled colloidal assembly

When TPM is mixed with the patched MIL-96 particles (2.9 ± 0.1 μm), it forms small oil droplets that selectively adhere and wet the patches of the particles. This produces a triblock soft-rigid-soft building block, shown in Fig. 3 (A and C), where the MOF particle is sandwiched by two TPM droplets/layers. TPM only sticks to the UiO-66 patches rather than the MIL-96 surface, presumably due to different surface charges/composition (see note S2). The molecular structures of the interfaces between TPM oil, the UiO-66 patch, and

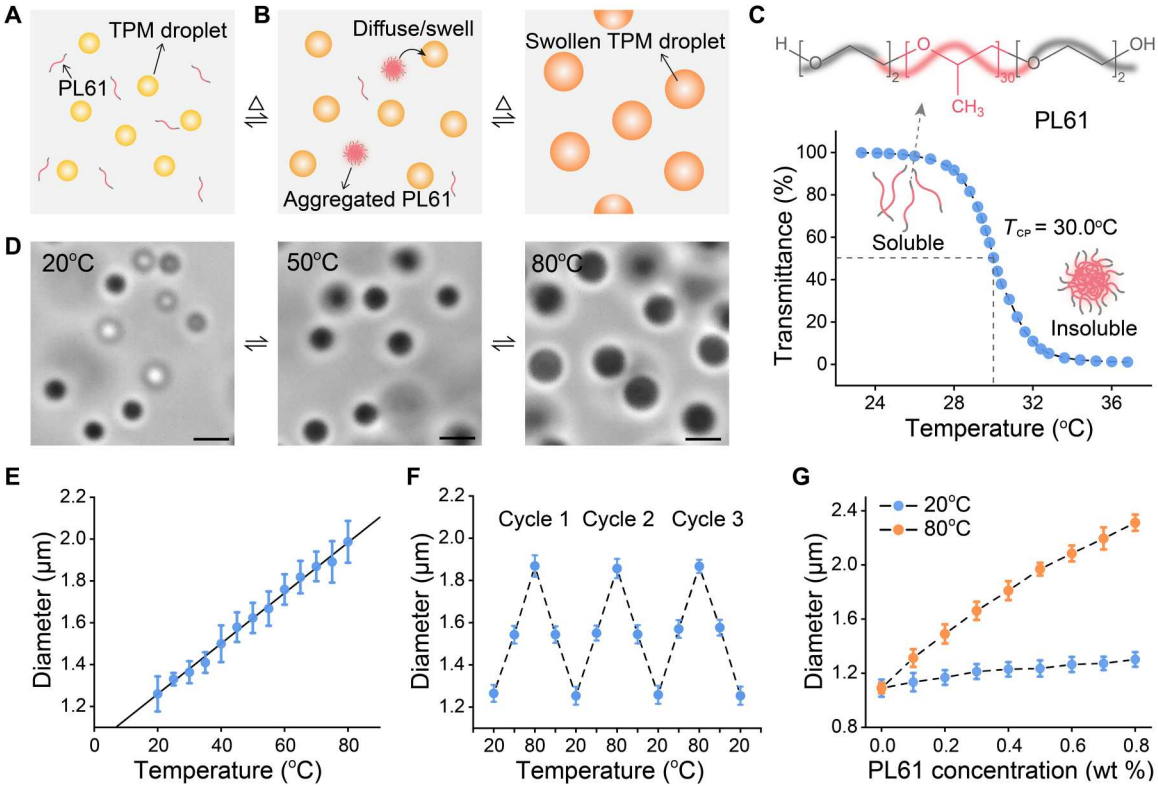

Fig. 2. The soft component. (**A**) Schematics of TPM oil droplets (spheres) and the swelling agent Pluronic L61, or PL61. (**B**) Size of TPM oil droplets changes upon heating/cooling by swelling/deswelling. (**C**) Top: Chemical structure of PL61. Bottom: Transmittance of PL61 aqueous solution containing 20% DMF as cosolvent, indicating the solubility of PL61 at different temperatures. The insets illustrate the soluble PL61 polymers at low temperatures and their aggregates at high temperatures. The cloud point temperature (transmittance = 50%) is around 30.0°C. (**D**) Microscope images showing the temperature-dependent size changing of micrometer-sized TPM droplets with 0.5 wt % of PL61. (**E**) Plot showing the diameter of TPM droplets versus temperature. (**F**) Plot showing the reversible thermal expansion and shrinkage of TPM droplets. (**G**) Plot of size of TPM droplets as a function of PL61 concentration at 20° and 80°C. Scale bars, 2 μm.

the MIL-96 particle are shown in Fig. 3D, whereby the UiO-66 patch bridges the soft (TPM oil) and rigid materials (MIL-96); it resembles the structure and role of endplate in human spine (Fig. 1). The thermoresponsive swelling/deswelling property of the TPM oil droplets on the triblock building block is confirmed. With PL61 and at varying temperatures, the TPM can expand and shrink accordingly (Fig. 3, A and C, and movie S2). During these processes, the TPM oil remains wetting on the patches of the MOF particle.

The triblock building blocks are further assembled to construct the MicroSpine, whereby the TPM droplets on different MOF particles merge to bridge the particles by liquid capillary force (Fig. 3, E and F). In forming the target linear alternating structure, the binding valence should be restricted to two (n = 2). For each MOF particle, the two patches allow specific interaction with two TPM oil lobes (Fig. 3A). While for the TPM, the valence is limited by reducing the volume of TPM oil on MOF particle, so only a thin film is formed (Fig. 3E). Merging of the thin films is only geometrically allowed between two particles (n = 2) but not more. This is easily controlled by adjusting the amount of TPM added to the system (Fig. 3G and see Materials and Methods). Linear colloidal chain with alternating soft-hard arrangement is assembled, being the MicroSpine, as shown is Fig. 3 (H to K). The chains upon formation can adopt a straight conformation (see also fig. S4). By introducing dye molecules, rhodamine B, the TPM films are visualized, which have uniform thickness (b) along the chain (Fig. 3, H and I). We can also solidify the TPM film, allowing for the characterization of the chains by scanning elelctron microscope (SEM) (Fig. 3J). Notably, the MOF particles in the chains have their side facets mutually aligned, which, by completely overlapping their hexagonal patches, maximizes the TPM-induced capillary force between particles.

We have examined the length distribution of the MicroSpine chains, and the result is shown in fig. S5. The relation between the number of particles per chain, x, and their weight fraction, w_x, can be fitted to the Flory-Schulz distribution, $w_x = x(1-p)^2 p^{x-1}$, where p is the extent of assembly. This indicates a step-growth assembly kinetics. The dispersity of the chains is estimated as $Đ = 1 + p$ and, for the specific sample shown, $Đ = 1.84$. We note that, compared to top-down method, MicroSpine chains are formed in solution, so that they can be produced in scalable yield (see also fig. S5).

While the linear structure is our target, branched structures (n > 2) can also be produced when the valence of TPM joints is not strictly controlled, for example, with an increased volume of the TPM oil. Some branched chains are shown in fig. S6, which are also used for special purposes (see the "Guest loading and release" section).

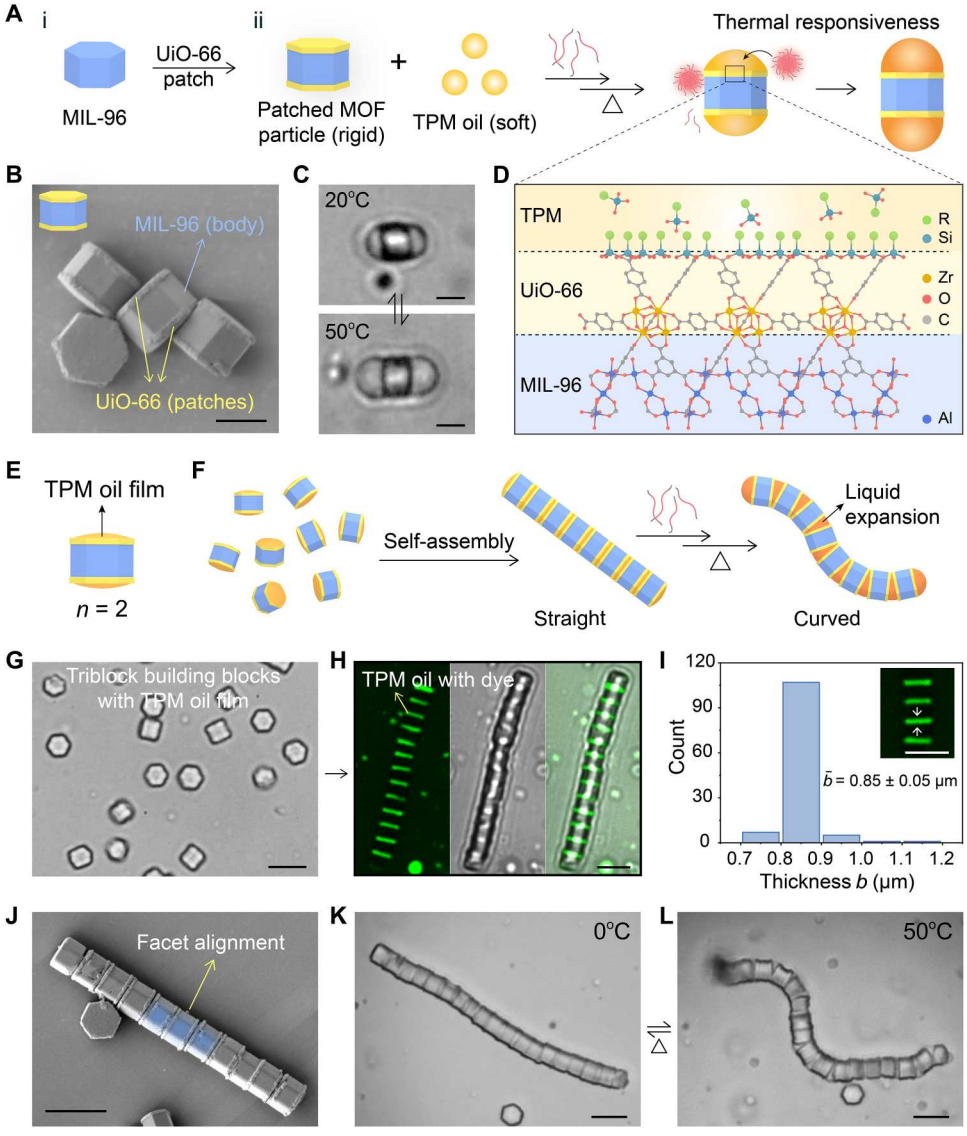

Fig. 3. The hard component and the assembly. (**A**) Schematics showing the patched MOF particle derived from MIL-96 hexagonal cylinder (i). TPM oil attaches and wets on the patches of MOF particle, forming a triblock soft-rigid-soft building block. With PL61 and upon heating, the TPM oil on the MOF particle can swell and expand, demonstrating their thermo-responsiveness (ii). (**B**) Scanning electron microscope (SEM) image of the patched MOF particles. The cylindric matrix (MIL-96) and thin patch (UiO-66) are indicated by blue and yellow arrows, respectively. (**C**) Microscope images showing the size changing of TPM oil attached to a MOF particle at 20° and 50°C. (**D**) Illustration of the molecular structures of the interfaces between TPM oil, UiO-66, and MIL-96. The UiO-66 is the key layer that bridges the soft TPM oil and hard MIL-96 particles. Green, cyan, orange, red, gray, and blue spheres represent organo-functional group of TPM, silicon, zirconium, oxygen, carbon, and aluminum atoms, respectively. (**E**) Cartoon showing thin films of TPM oil formed on the UiO-66 surface to reduce assembly valence ($n = 2$). (**F**) Schematics showing the assembly of linear chain and its thermoresponsive shape changing through liquid expansion. (**G**) Microscope images of the triblock building blocks with thin TPM oil films before self-assembly. (**H**) Confocal fluorescent and bright-field microscope images of an assembled colloidal chain, with the TPM oil films doped with rhodamine B dye molecules. (**I**) Histogram showing the distribution of the thickness of TPM film (b). (**J**) SEM image with false color showing the mutually aligned facets of MOF particles after assembly. (**K** and **L**) Microscope images of a representative chain with straight/curved conformations at 0° and 50°C. Scale bars, 2 μm (B) and (C) and 5 μm (G) to (L).

Thermoresponsive actuation of MicroSpine

With PL61 and upon heating, the MicroSpine transforms from the straight state to a curved state (Fig. 3, K and L). This is due to the expansion of the TPM parts, which spaces the MOF particles further apart and allows some adjacent MOF particles to adopt a non-aligned orientation. This local flexibility builds up along the chain and results in the chain's global shape transformation. When the system is cooled, the chain returns to the straight state, as the TPM joints shrink and resume the film state, which forces the MOF particles to come close and overlap their flat patch facets.

Microscope images in Fig. 4A and movie S3 show the reversible shape changing (or actuation) of a MicroSpine chain in a heating-cooling cycle. The chain's conformation is characterized by its end-to-end distance (R^e), and its temperature dependence is further investigated by recording R^e values at 5°C intervals. As shown in Fig. 4B, R^e decreases only slightly at the beginning of a heating

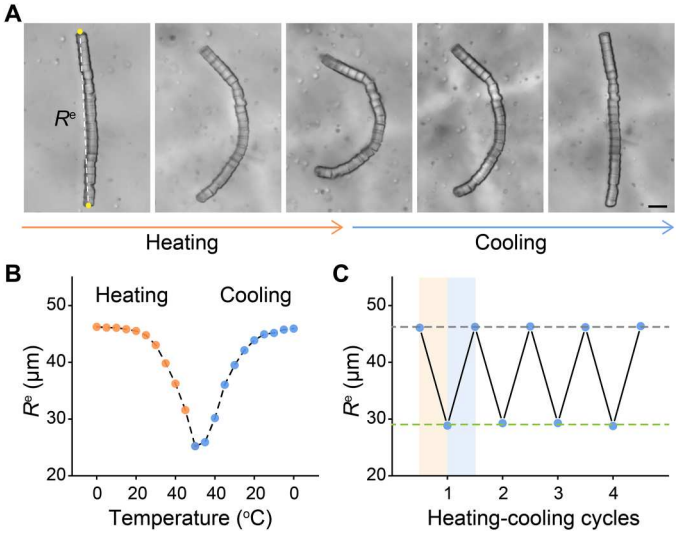

Fig. 4. Thermoresponsive actuation of MicroSpine chain. (**A**) Microscope images of a representative MicroSpine chain during a heating/cooling cycle. The chain transforms from straight to curved and then back to straight conformations. (**B**) Plot of the chain's end-to-end distance R^e over temperature, which decreases upon heating (orange dots) and increases on cooling (blue dots). (**C**) Shape transformation of MicroSpine chains, characterized by R^e, is reversible and is performed for four cycles. The gray and green dotted lines delineate the fully straight and bent states, respectively. The pale orange and pale blue shades represent heating and cooling processes, respectively. Scale bar, 5 μm.

cycle. This is because the small volume change of the TPM joints has yet to contribute to the curvation of the chain; because of favorable wetting, TPM still induces strong capillary force between flat surfaces of bound MOF particles. A sharp decrease of R^e starts at around 30°C, signifying a large shape changing of the chain. Likewise, when cooling the chain down from 50° to 0°C, R^e increases accordingly. We note that these heating-cooling cycles can be repeated reversibly for many times (Fig. 4C). The shape transformation occurs quickly, within several seconds, after heating or cooling the chains (see fig. S7 and movie S4 for more information).

The shape transformation of MicroSpine, ascribed to the swelling-induced volume expansion/shrinkage of the TPM oil at the corresponding temperatures, can also be regulated by the concentration of PL61. Microscope images in Fig. 5A show the representative chains of similar lengths at 50°C, while the amount of PL61 varies, from 0 to 0.4 wt %. Without PL61, the chains do not show responsiveness and remain straight at high temperatures. Adding a small amount of PL61, 0.025 to 0.1 wt %, leads to moderate bending between the chain segments. More flexible, curved chains with various conformations can be obtained by further increasing the PL61 concentration from 0.2 to 0.4 wt %.

For MicroSpine chains, we define the bond vector, **r**, as one that connects the centers of two TPM joints and passes through the centre of the sandwiched MOF particle, as illustrated in Fig. 5B. The angle between adjacent bonds is the bond angle, θ. At each of PL61 conditions, the values of θ for around 20 individual chains are collected. The distributions of |θ| are shown in Fig. 5B and fig. S8, which normally follow a Gaussian form (see note S3). With a rise in PL61 amount from 0.05 to 0.4 wt %, the mean value of θ shifts from 10° to 36°, indicating a larger allowed curvation at each MOF-TPM junction. The broad distribution of θ at the higher PL61 concentrations corresponds to a greater chain flexibility. For example, at 0.4 wt % of PL61, the chain at 50°C is almost completely collapsed (Fig. 5A, bottom right). We also show that MicroSpine chains assembled from MOF particles with a truncated hexagonal bipyramid shape, and a small patch can entertain increased chain flexibility, as shown in fig. S9. This is attributed to a relatively thick TPM film sandwiched between two MOF particles.

The flexibility of MicroSpine chains can also be quantified. Within each chain, the bond vector freely rotates in two-dimensional (2D), as illustrated in Fig. 5B and fig. S10. This assumption ignores the out-of-plane chain twisting, which, due to the gravity of the chain, is only occasionally observed in experiments (see also note S3). In addition, because the TPM joints are of similar sizes, we assume that all bond lengths (equal to r) are identical at the same conditions. We apply the 2D worm-like chain model (*38*) (commonly used for linear polymers) to derive the persistence length (l_p) of MicroSpine chains, as also shown in Fig. 5B. For the chain confined in 2D, the degree of flexibility is determined by the orientation correlation function, denoted as $\langle\cos\theta_{(s)}\rangle$. This function represents the mean cosine of the bond angles between different bond vectors ($\mathbf{r}_i$ and $\mathbf{r}_j$, $1 \le i < j \le m$) separated by the arc length s. Here, $\theta_{(s)}$ is the angle change over s, while m is the total number of bonds per chain. The arc length s can be approximated by $s = r(j - i + 1)$ and runs from 0 to the contour length of the MicroSpine chain denoted by l ($l = mr$). This correlation can be described as an exponential function

$$\langle\cos\theta_{(s)}\rangle = \exp\left(-\frac{s}{2l_p}\right) \quad (1)$$

Equation 1 can be rewritten as

$$\langle\cos\theta_{ij}\rangle \approx \exp\left(-\frac{j-i+1}{2s_p}\right) \quad (2)$$

where $s_p = l_p/r$ represents the number of bonds in the persistence segment, and it is also the property of chain flexibility as used in this context. Taking the natural logarithm on both sides of Eq. 2, s_p can be estimated by extracting the slope of the equation (see note S3 for more details).

The values for s_p at PL61 concentrations of 0 to 0.5 wt % are shown in Fig. 5C. As can be seen, a notable decrease in s_p, from 830 to 24, occurs when PL61 concentration increases from 0 to 0.05 wt %. This is followed by a relatively slow decline to $s_p = 11$ at 0.1 wt % of PL61, while further increase in PL61 amount only gives a slight reduction to $s_p = 1.7$ at 0.5 wt %. For linear chains of an organic polymer, it is denoted as rigid, semiflexible, and flexible when the ratio between the contour length and the persistence length l/l_p is $\ll 1$, ~1, or $\gg 1$, respectively. Similarly, we define the degree of flexibility of MicroSpine chain as f, which is given by m/s_p. We calculated the average value of f for 20 chains under each condition, shown in Fig. 5C. The MicroSpine is accordingly classified as rigid, semiflexible, and flexible when PL61 concentration is <0.05, 0.05 to 0.1, and >0.1 wt %, respectively.

Tuning actuation behaviors by photopatterning

Because TPM oil droplets can be solidified by photopolymerization (in presence of photoinitiators) and they are in alternating locations

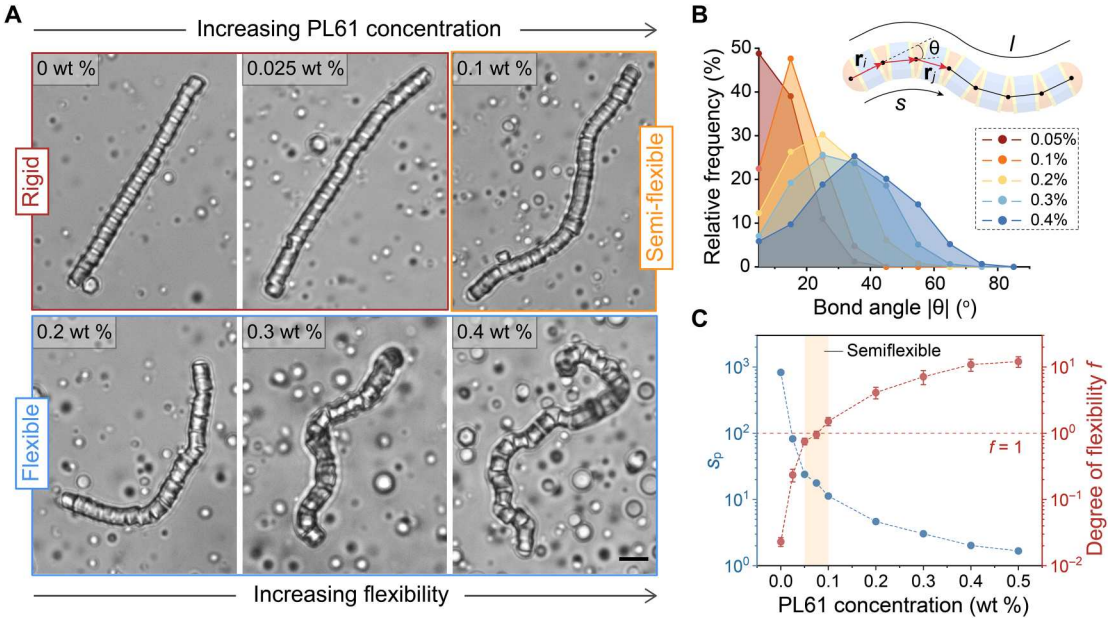

Fig. 5. Conformations of MicroSpine. (**A**) Microscope images of MicroSpine chains at 50°C, with various concentrations of PL61 (0 to 0.4 wt %). Iron red, orange, and blue frames represent rigid, semiflexible, and flexible conformations. (**B**) Probability of bond angles |θ| for MicroSpine chains at different conditions. The inset depicts the chain model, highlighting the bond vector **r**, bond angle θ, separating arc length *s*, and chain's contour length *l*. (**C**) A plot illustrates the effect of PL61 concentration on the shape transformation of MicroSpine chains, with the blue dots representing the calculated number of bonds in the persistence segment (s_p) and the red dots showing the corresponding degree of chain flexibility (*f*). The orange shading indicates the classified semiflexible conformations. Scale bar, 5 μm.

along the MicroSpine chain, we seek to realize a more controlled actuation by selectively hardening the TPM joints. In other words, we can design by patterning the number and location of the soft segments within a chain. We use an ultraviolet (UV) laser (built within a customized microscope) with variable beam sizes comparable to the particle sizes, around 4 to 20 μm in diameter, which allows us to cure the TPM droplets one at a time or as a group (Fig. 6, A and B, and see Materials and Methods and fig. S11 for microscope setup). The solidified TPM joints become rigid and thus lose their response to heating.

For example, Fig. 6 (C to E) and movie S5 show the sequential photomanipulation of a MicroSpine chain, which contains 22 TPM parts, and the corresponding actuation behaviors. Initially, this chain was straight at 0°C with all bond angles |θ| < 10°. When

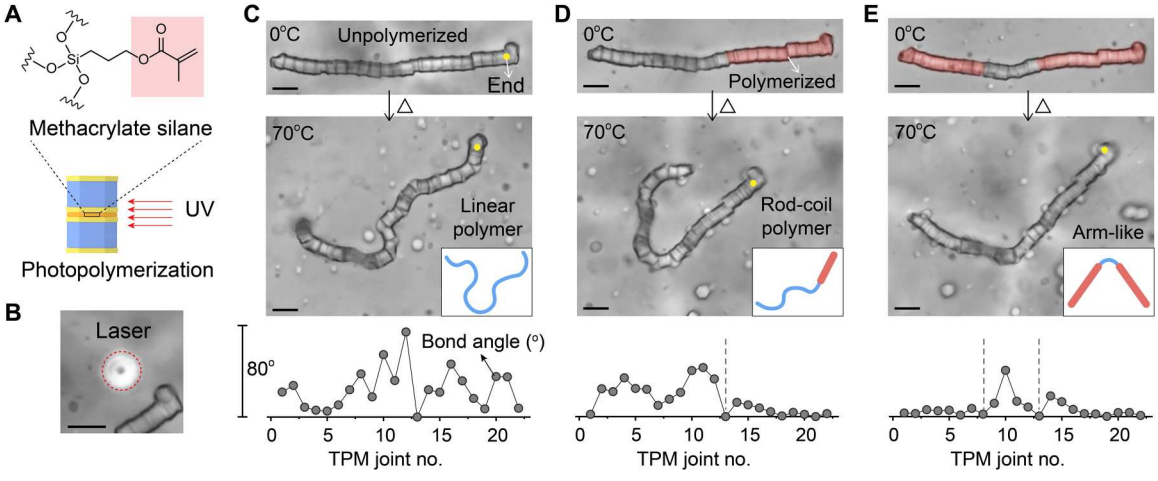

Fig. 6. Photopatterning of MicroSpine chain. (**A**) Schematic showing that the TPM joint can be polymerized by UV irradiation (red arrows). The zoomed-in view shows the molecular structure of TPM oil. (**B**) Microscope image showing the laser spot (beam width about 4 μm) used for photopolymerization, highlighted by dotted circle. (**C**) Microscope images showing a MicroSpine chain in straight conformation at 0°C and curved conformation at 70°C, which imitates linear polymer (inset) in a good solvent. The plot shows the bond angles as a function of TPM joint number along the chain at 70°C. The yellow dot represents the last TPM joint of the chain. (**D** and **E**) Top: Microscope images showing the blocks of the chain in (C) irradiated at 0°C (in red), which become rigid and unresponsive to heat. Middle: Microscope images of the chain when heated to 70°C. The chain is partially responsive and forms a rod-coil "polymer" (D) and a colloidal "arm" (E), respectively. The bottom graphs are the corresponding bond angle distributions along the chain. Scale bars, 5 μm.

heated to 70°C, it transforms into a flexible chain with a wide distribution of bond angles, $|\theta| \leq 75°$, as shown in Fig. 6C.

Then, as a proof of concept, the last 10 TPM oil parts (shown in red) are cured by UV laser irradiation for several minutes at 0°C. When reheated, the treated chain block becomes rigid, defying shape transformation. Consequently, MicroSpine can be viewed as a rod-coil colloidal copolymer (Fig. 6D). Likewise, an arm-like shape, shown in Fig. 6E, has been achieved by rigidifying the first eight soft segments (at 0°C), leaving four TPM oil joints in the middle contributing to the arm bending. The bond angle $|\theta|$ as a function of particle position is also displayed for each morphology. In principle, the laser-induced photopolymerization can be used to create more precise locations and complex actuation patterns of MicroSpine. For instance, the curing time can be controlled so the relative rigidity of each TPM joint may be regulated.

Guest loading and release

Having shown the thermoresponsive actuation of MicroSpine, we then demonstrate its potential in executing simple tasks. Colloidal capsules, which can open and close in response to temperature, are designed to capture and release colloidal guests (e.g., cargos) (Fig. 7A). In one case, a MicroSpine chain consisting of 17 MOF particles is manually selected, which upon moderate heating (50°C) bends toward one side to form an open cavity, as shown in Fig. 7 (A and B) and movie S6. We use a TiO_2 microbead 8.0 μm in size as the guest, which can be guided by UV laser to move toward the capsule by negative phototaxis (*39*). The TiO_2 upon partially irradiation can induce photocatalytic reactions on its surface, which results in unbalanced ion gradients around the particle that propel the particle away from the laser by diffusiophoretic motion (see also fig. S12). Consequently, the TiO_2 bead can propel (or swim) and enter the cavity of MicroSpine.

In another case, we use a branched MicroSpine chain to demonstrate guest entrapment and release, and the process is shown by microscope images in Fig. 7C. A P-shaped structure consisting of two chains is selected, as it is geometrically possible to produce a close cavity. At 80°C, the structure has a narrow channel of width w = 1.8 μm, labeled in Fig. 7C, which keeps the TiO_2 microbead (d_{TiO2} = 6.8 μm) outside of the cavity. By adjusting the temperature, the channel width w adopts four stages. As shown in Fig. 7 (C and D) and movie S6, when cooling to 40°C, the channel opens slowly with an increasing w by shrinking the TPM oil (stage 1, w = 7.2 μm). The width of channel remains constant at 40°C, so that the TiO_2 microbead can move and enter the cavity guided by the laser (stage 2, $w \sim 7.5$ μm). Subsequently, the TiO_2 bead is trapped by a closure of the cavity through a temperature rise (stage 3, w = 0.3 μm at 80°C). To release the guest, the system is cooled to 0°C (stage 4, $w \gg d_{TiO2}$).

Last, we show that a branched MicroSpine can collect two particles. As shown in Fig. 7E and movie S7, two TiO_2 microbeads, 5.5 and 6.5 μm, are sequentially trapped when the branched structure collapse inward at increasing temperatures.

DISCUSSION

We have introduced a soft-hard microactuator (MicroSpine) with shape-changing properties by hybridizing rigid MOF particles and responsive oil droplets via colloidal assembly. The actuators can reversibly transform between different conformations through a swelling/deswelling mechanism, well controlled by temperature and the concentration of swelling agent. We have also shown the system's ability to encapsulate and release colloidal objects.

Although MicroSpine becomes flexible by TPM swelling, this mechanism does not precisely decide what shape the chains may deform into. In alleviating this issue, we have demonstrated photopatterning, which leads to a more controllable shape transformation. With a customized setup, it is possible to gain independent control over the selected joints to realize more complicated actuations.

While the shape of human spine is regulated by a complex interplay of various biological structures including muscles, spinal cord, and nervous system, external forces may be introduced in the future to fully manipulate MicroSpine. Light, electric, and magnetic field can be used for chains functionalized with smart materials, such as gold and magnetic nanoparticles (*26*, *40*–*42*), while MOF provides a suitable platform to include functional materials and molecules (*43*, *44*). For example, we have revealed this possibility by synthesizing Fe_3O_4-modified MOF particles and subsequently assembling them into MicroSpine. Guided by an external magnetic field, the MicroSpine chain can rotate and translate (see more details in figs. S13 and S14 and movie S8). Ultimately, optical tweezers with multiple traps can be used to control the shape of the chains.

The use of colloidal assembly for making actuators represents an important step toward creating complex microscale devices or robotics. In macroscale, sophisticated machines are assembled by many mechanical parts. Colloidal co-assembly has the potential to combine nano- and microscale building components of various kinds, and the process is spontaneous, simple, and high yielding. Although necessary information needs to be encoded into colloidal particles for their assembly and actuation, the rapidly developing field of colloidal synthesis can facilitate these efforts (*45*).

Biological system has always been a source of inspirations for man-made systems. In our work, through rational design, the MicroSpine microactuator not only emulates the structure of spine, with alternating soft and hard segments, but also mimics the swelling/deswelling mechanism of the spinal discs for shape transformation. Following this strategy, we anticipate the translation of other biological workings to artificial microscale systems, possibly built through colloidal assembly.

MATERIALS AND METHODS

Materials

TPM (98%) and azobisisobutyronitrile (AIBN, 98%) were obtained from Sigma-Aldrich. Ammonia (28%), aluminum nitrate nonahydrate [$Al(NO_3)_3 \cdot 9H_2O$, 99.5%], 2-aminoterephthalic acid (NH_2-H_2bdc, 98%), caprylic acid (98%), and the photoinitiator, 2-hydroxy-2-methylpropiophenone (98%) were purchased from Energy Chemical. PL61 (number-average molecular weight, ~2000) was purchased from Aldrich Chemistry. 1,3,5-benzenetricarboxylic acid (H_3btc, 99%), tetrabutyl titanate (TBT: 99%), SDS (99%), and rhodamine B (99%) were purchased from J&K Scientific Ltd. Zirconium (IV) oxide chloride octahydrate ($ZrOCl_2 \cdot 8H_2O$, 98%), hydroquinone (99%), iron(II) chloride tetrahydrate ($FeCl_2 \cdot 4H_2O$, 99%) were purchased from Dieckmann Chemicals. Iron(III) chloride hexahydrate ($FeCl_3 \cdot 6H_2O$, 99%) was obtained from Alab (Shanghai) Chemical Technology Co. Ltd. The D5 dye,

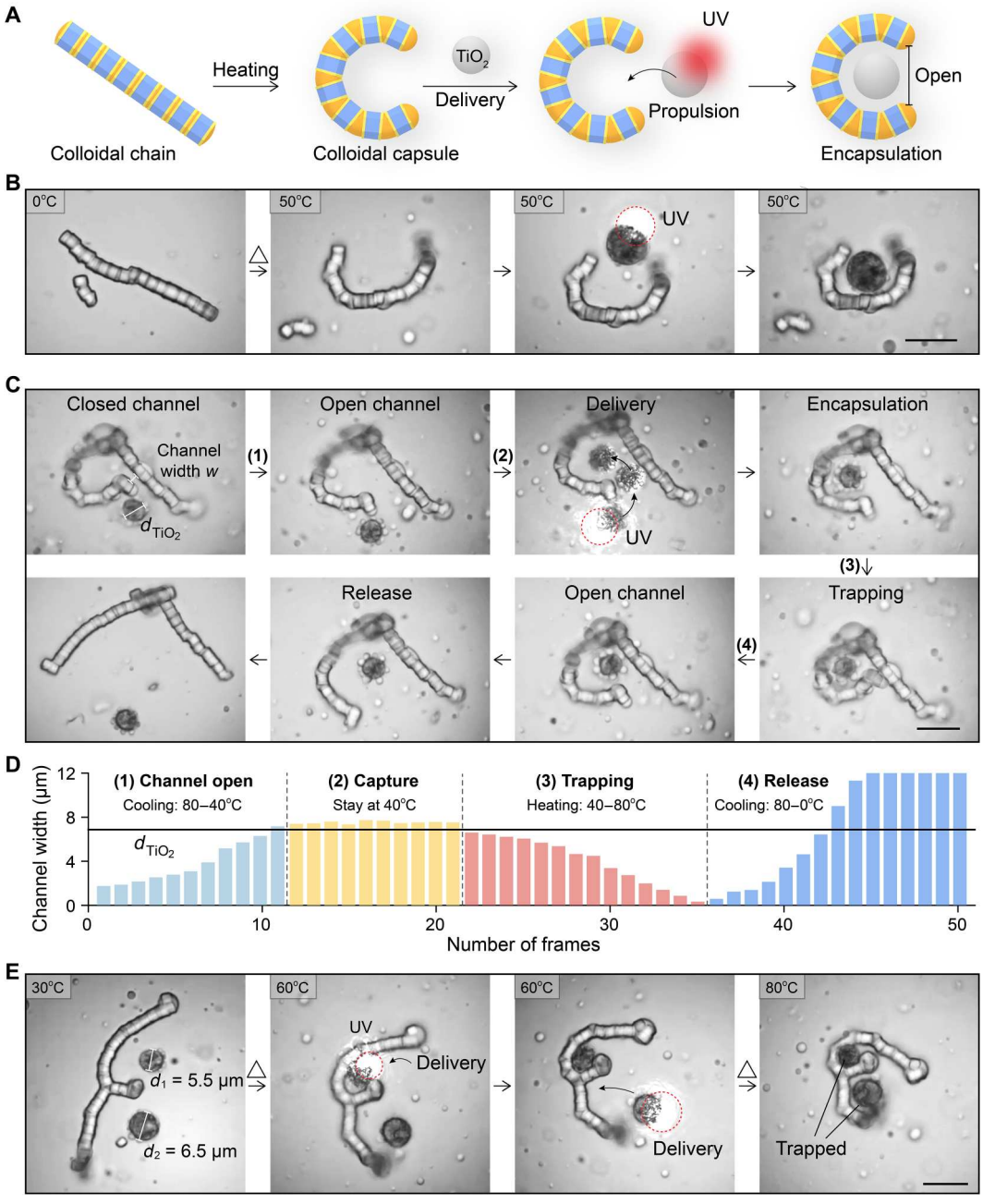

Fig. 7. Guest capture and release. (**A**) Schematics show that the actuation of MicroSpine chain can be used to capture colloidal guests (TiO_2 microbeads, gray spheres) with its cavity. The microbead is guided by UV laser (red shade) to enter the colloidal capsule. (**B**) Snapshots from a movie show a linear chain forming a capsule and capturing a TiO_2 microbead (8 μm) at 50°C. (**C** and **D**) Microscope image series in (C) show the successive capture and release of TiO_2 microbead (6.8 μm) by a branched chain adopting a P shape. The width *w* of the opening for the capsule is highlighted, which can be programmed by temperature. The diameter of TiO_2 microbead is also labeled. The image was superimposed to show the trajectory of TiO_2 during delivery. Graph in (D) shows the channel width over video frames. The programmed four stages are shown in different colors. The black line delineates the diameter of TiO_2 microbead. (**E**) Microscope images showing the sequential capture of two TiO_2 microbeads by a branched chain. The diameters of two microbeads are shown. The red dotted circles on the microscope images show the locations of UV laser. Scale bars, 10 μm.

3-{5-[4-(diphenylamino)styryl]thiophen-2-yl}-2-cyanoacrylic acid (>95%) was purchased from Dyenamo. Other chemicals include acetic acid (HAc; 99.7%; Chemicals Duksan), polyvinyl alcohol (98 to 99%; Alfa Aesar), benzoquinone (99%; Acros Organics), and hydrochloric acid (HCl; 37%; RCI Labscan Ltd).

Methods

Synthesis of TPM droplets

TPM oil droplets about 1 μm in diameter were synthesized by the hydrolysis and condensation reaction of TPM in water. Typically, 25 μl of TPM and 10 μl of ammonia (28%, wt %) were added into 5 μl of deionized (DI) water. The mixture was stirred at 150 rpm for 20 hours to allow complete reaction, after which the suspension became milky, and uniformly sized TPM oil droplets were formed. Then, DI water, DMF, and 2 wt % of PL61 were added dropwise in the suspension, with continuous mixing at a vortex mixer (~3000 rpm). The suspension was diluted by five times, and DMF concentration was kept at 20% (v/v). The PL61 was varied from 0 to 0.8 wt % to study its effect on the behavior of thermoresponsive size changing of the TPM oil droplets while keeping the number of oil droplets constant.

Synthesis of MOF particles

The patched MOF particles were fabricated using a seeded growth protocol we reported before (*37*), with modifications. MIL-96 microcrystals were first synthesized as the seed particles using a solvothermal procedure. For the cylindrical MIL-96 particles 2.9 ± 0.1 μm in size, 4.0 g of $Al(NO_3)_3{\cdot}9H_2O$ and 1.05 g of H_3btc were dissolved in 40 ml of DMF/H_2O (1:4, v/v), to which 10 ml of HAc was added. The mixture was sealed in an autoclave and heated at 130°C in the oven for 24 hours. Then, the produced MIL-96 seed particles were washed three times by centrifugation/redispersion with DMF and were stored in 50 ml of DMF.

Similar procedures were followed to synthesize MIL-96 seed particles with other shapes or sizes. The truncated hexagonal bipyramid-shaped particles were fabricated by dissolving 1.0 g of $Al(NO_3)_3{\cdot}9H_2O$, 0.5 g of H_3btc, 0.3 ml of HAc, and 0.2 ml of DMF to 8 ml of DMF/H_2O (1:4, v/v), followed by heating at 210°C for 18 hours. To synthesize the cylindrical MIL-96 particles 1.8 ± 0.1 μm in size, a 40 ml of solution containing $Al(NO_3)_3{\cdot}9H_2O$ (25 mg/ml) and H_3btc (15 mg/ml) in 1:3 DMF/H_2O was prepared and 10 ml of HAc was added. The mixture was heated at 150°C for 24 hours to obtain the desired particles. In all cases, the synthesized particles were washed by centrifugation/redispersion cycles with DMF.

The MIL-96–UiO-66 MOF particles were synthesized by mixing 400 μl of MIL-96 seed particle suspension with 150 μl of NH_2-H_2bdc in DMF (25 g/liter), 150 μl of $ZrOCl_2{\cdot}8H_2O$ in DMF (10.5 g/liter), and 400 μl of HAc in a glass vial. The mixture was heated at 90°C and agitated in a shaker with a thermostat for 3 hours. The MOF particles were then washed three times with DMF and stored in 500 μl of DMF.

Synthesis of TiO_2 microbeads

The TiO_2 microbeads were synthesized using an oil-in-water microemulsion method (*46*). Typically, 2 ml of caprylic acid solution with 10 wt % of titania precursors (TBT) as an oil phase was added into a 40 ml of polyvinyl alcohol (2 wt %) aqueous solution. Upon magnetic stirring, oil-in-water emulsion formed where the TBT and caprylic acid oil microdroplets dispersed in the aqueous solution. Then, 4.5 ml of ammonia (28 wt %) was added to trigger the hydrolysis of TBT. The solution was left standing still for 24 hours before it was kept stirring for another 5 min. The produced TiO_2 microbeads were washed three times with ethanol using the centrifugation/redisperse cycles. The dye-sensitized TiO_2 microbeads were prepared by immersing the beads in a 0.8 mM ethanolic D5 dye solution for about 2 hours to complete the dye absorption, according to our previous protocol (*38*).

Synthesis of Fe_3O_4@MOF particles

Cylindrical MIL-96-UiO-66 MOF particles, with an average size of 1.8 ± 0.1 μm in size, were functionalized with Fe_3O_4 magnetic nanoparticles. Briefly, 600 μl of MIL-96–UiO-66 MOF particles in DMF was centrifuged and dried at 80°C for 12 hours. A stock solution was then prepared by mixing 82.5 mg of $FeCl_3{\cdot}6H_2O$, 30.4 mg of $FeCl_2{\cdot}4H_2O$, and 12.7 μl of HCl (12 M) with 3 ml of DI water. Then, the dried MOF particles were immersed in 1.5 ml of the freshly made stock solution for 8 hours, followed by heating at 80°C for 1 hour. Subsequently, 480 μl of 4.2 wt % of ammonia solution was added to the suspension and stirred for 5 min. The resulting dark particles were collected and washed with DI water until pH became neutral and afterward washed with DMF for several times. The Fe_3O_4@MOF particles can be purified by removing the Fe_3O_4 nanoparticles through centrifugation at 3000 rpm and lastly were stored in 500 μl of DMF.

Self-assembly of MicroSpine

The soft-hard structure of MicroSpine upon assembly consists of TPM thin film and MOF particles (UiO-66–patched MIL-96 particle). To achieve the TPM thin film, 20 μl of TPM was prehydrolyzed in 5 ml of DMF/H_2O (2:3, v/v) for 2 days. Then, a stock solution was prepared by mixing 500 μL of prehydrolyzed solution with 19 μl of aqueous SDS (1%, w/w) and 6.4 μl of ammonia (5.6%, w/w). For the combination of soft and hard components, 20 μl of MOF particle suspension in DMF was added to 100 μl of freshly made stock solution in a 2-ml plastic Eppendorf tube. For the triblock soft-rigid-soft building blocks, the mixture was left still for 2 hours; for the colloidal chains with alternating structure, it was gently stirred at 250 rpm for 1.5 hours. Samples at different assembly times were observed under a microscope to examine the initial shape of the colloidal chains. Fe_3O_4@MOF particles were assembled using the same protocol to achieve the MicroSpine chains that can respond to an external magnetic field.

To image the TPM oil layers within the chain structure, 2 μl of rhodamine B solution (0.1 g/liter) was mixed with 20 μl of the above colloidal chain suspension. To characterize the chain structure by scanning electron microscopy, the chains were solidified by adding 1 mg of AIBN initiator to the system and polymerizing the TPM oil at 80°C in the oven for 2 hours. The solidified chains were collected by repetitive centrifugation and redispersion with DMF.

To investigate the thermoresponsive shape-changing properties, DI water, DMF, and 1 wt % of PL61 were added dropwise to the 120 μl of suspension containing the triblock soft-rigid-soft building blocks or the assembled colloidal chains. For a typical demonstration of thermoresponsive shape changing, the DMF was kept at 20% (v/v) in water and the PL61 were kept and 0.3 wt %, respectively. The sample used to achieve precise actuation by photopatterning contains an additional 0.5 M photoinitiator, 2-hydroxy-2-methylpropiophenone, which can diffuse into the TPM thin films within minutes. To investigate the influence of PL61 amount, its

concentration was varied from 0 to 0.5 wt %, while other factors were kept constant.

Thermoresponsive shape changing

The above suspension containing soft TPM droplets, triblock hybrids, or MicroSpine structures was charged and sealed in a rectangular glass capillary tube (20 mm by 2.00 mm by 0.10 mm), which was mounted on a heating stage (Instec mK2000 or Linkam LTS420) fitted to an optical microscope. The temperature was varied and monitored. Reversible size/shape changes were observed on microscope when the temperature of the sample was adjusted. The samples were held isothermally for over 2 min at each temperature before images and videos were taken.

To investigate the response time of MicroSpine chains to temperature, the sample was heated at a ramp rate of 30°C/min until it reached 80°C. It was held at 80°C for 30 s before being cooled at the same rate until it reached −10°C.

Photopatterning on the MicroSpine

A home-built microscope with bright-field and size-tunable UV laser beam (4 to 20 μm in diameter) was designed, as illustrated in fig. S7. The single-spot UV beam can selectively cure the TPM joints in the MicroSpine by photopolymerization (in the presence of a photoinitiator). Before UV radiation, the sample containing colloidal chains was cooled to around 0°C. Then, the laser spot was moved to the desired position of a chain under the bright field, followed by a 6-min radiation to solidify the soft components. The size of laser spot was tuned depending on the number of the soft segments needed to be solidified.

Guest encapsulation

The D5-sensitized TiO_2 microbeads were dispersed in a solution containing 20 mM hydroquinone and 10 mM benzoquinone. Then, 33 μl of the above solution was mixed with 12 μl of PL61 (1 wt %) and 5 μl of the suspension containing MicroSpine structures. The mixture was loaded in a rectangular glass capillary tube and fixed on the heating stage, which is mounted on the home-built microscope equipped with the size-tunable UV laser beam described above. Microcapsules formed or disappeared by heating or cooling the sample. Then, beam width of the UV laser was adjusted to ~7 μm in diameter, which was used to direct the motion of TiO_2 microbeads toward the MicroSpine capsule.

Magnetic field-responsive MicroSpine chains

The colloidal chains assembled from Fe_3O_4@MOF particles was charged in a capillary tube for microscope observation. A bar magnet was brought close to the sample and used to manipulate the chains, inducing both rotational and translational motions.

UV-visible spectroscopy

The thermoresponsive phase separation of PL61 in DMF/H_2O cosolvent system was characterized by measuring the change in transmittance of the solution at different temperatures using UV-vis spectroscopy. The experiment was conducted on an Agilent Cary 60 spectrophotometer equipped with a Peltier single-cell holder (0° to 100°C). L61 (0.5 wt %) was dissolved in the cosolvent with different DMF percentages (0° to 40%, v/v), which was then charged in a quartz cuvette. The experiment started with a heating step from ~20° to ~40°C at a rate of 0.2° to 0.8°C/min. The sample was equilibrated at each desired temperature before measuring the absorbance at 600 nm. For each sample, turbidimetry curve was obtained and the cloud point temperature T_{cp}, where the transmittance is 50%, can be measured.

Microscopy

TPM droplets, MOF particles, and their assemblies were observed on the home-built microscope with a Hikvision MV-CH050-10UM camera, or on a Leica DM2000 upright microscope with a MC170 camera, or on a Nikon Eclipse Ti-2 inverted microscope equipped with a Nikon D7000 DSLR camera. ImageJ was used to measure the diameter of TPM droplets, the end-to-end distance (R^e)/bonding angle of the MicroSpine structures, and the channel width of the microcavity. Confocal fluorescence microscopy of the MicroSpine was conducted on a Leica SP8 confocal laser scanning microscope. The MOF particles, Fe_3O_4@MOF particles, and TiO_2 microspheres in the dried state were imaged by a Tescan MAIA3 XMH scanning electron microscope at 2 kV using the secondary electron detector. Energy-dispersive x-ray spectroscopy was performed on Fe_3O_4@MOF particles at 15 kV. Some of the images were digitally post-processed to improve brightness and contrast.

Supplementary Materials

This PDF file includes:

Notes S1 to S3
Figs. S1 to S14
Legends for movies S1 to S8
References

Other Supplementary Material for this manuscript includes the following:

Movies S1 to S8

REFERENCES AND NOTES

1. K. V. Kardong, *Vertebrates: Comparative Anatomy, Function, Evolution* (McGraw-Hill Education, ed. 8, 2018).
2. H. A. L. Guerin, D. M. Elliott, *Structure and Properties of Soft Tissues in the Spine* (Academic Press, 2006).
3. C. F. Herreid, *Locomotion and Energetics in Arthropods* (Plenum Press, ed. 1, 1981).
4. D. H. Lynn, *The Ciliated Protozoa: Characterization, Classification, and Guide to the Literature* (Springer Netherlands, ed.3, 2008).
5. G. Runge, T. Preller, S. Zellmer, S. Blankemeyer, M. Kreuz, G. Garnweitner, A. Raatz, Spine-Man: Design of a soft robotic spine-like manipulator for safe human-robot interaction in *Proceedings of IEEE/RSJ International Conference on Intelligent Robots and Systems (IROS)* (IEEE, 2015), pp. 1103–1110.
6. S. Mintchev, J. Shintake, D. Floreano, Bioinspired dual-stiffness origami. *Sci. Robot.* **3**, eaau0275 (2018).
7. A. Nemiroski, Y. Y. Shevchenko, A. A. Stokes, B. Unal, A. Ainla, S. Albert, G. Compton, E. MacDonald, Y. Schwab, C. Zellhofer, G. M. Whitesides, Arthrobots. *Soft Robot.* **4**, 183–190 (2017).
8. Y. Chen, F. Wan, T. Wu, C. Song, Soft-rigid interaction mechanism towards a lobster-inspired hybrid actuator. *J. Micromech. Microeng.* **28**, 014007 (2017).
9. H.-C. Fu, J. D. L. Ho, K.-H. Lee, Y. C. Hu, S. K. W. Au, K.-J. Cho, K. Y. Sze, K.-W. Kwok, Interfacing soft and hard: A spring reinforced actuator. *Soft Robot.* **7**, 44–58 (2019).
10. S. Wu, Q. Ze, R. Zhang, N. Hu, Y. Cheng, F. Yang, R. Zhao, Symmetry-breaking actuation mechanism for soft robotics and active metamaterials. *ACS Appl. Mater. Interfaces* **11**, 41649–41658 (2019).
11. S. W. Kwok, S. A. Morin, B. Mosadegh, J.-H. So, R. F. Shepherd, R. V. Martinez, B. Smith, F. C. Simeone, A. A. Stokes, G. M. Whitesides, Magnetic assembly of soft robots with hard components. *Adv. Funct. Mater.* **24**, 2180–2187 (2014).
12. J. M. McCracken, B. R. Donovan, T. J. White, Materials as machines. *Adv. Mater.* **32**, 1906564 (2020).
13. H. Zhang, W. Yang, Q. Liu, Y. Gao, Z. Yue, B. Xu, Mechanical Janus structures by soft–hard material integration. *Adv. Mater.* **35**, 2208339 (2023).
14. E. Palleau, D. Morales, M. D. Dickey, O. D. Velev, Reversible patterning and actuation of hydrogels by electrically assisted ionoprinting. *Nat. Commun.* **4**, 2257 (2013).
15. L. Hines, K. Petersen, G. Z. Lum, M. Sitti, Soft actuators for small-scale robotics. *Adv. Mater.* **29**, 1603483 (2017).

16. H. Zeng, Y. Wang, T. Jiang, H. Xia, X. Gu, H. Chen, Recent progress of biomimetic motions —From microscopic micro/nanomotors to macroscopic actuators and soft robotics. *RSC Adv.* **11**, 27406–27419 (2021).
17. B. J. Nelson, I. K. Kaliakatsos, J. J. Abbott, Microrobots for minimally invasive medicine. *Annu. Rev. Biomed. Eng.* **12**, 55–85 (2010).
18. C. Hu, S. Pané, B. J. Nelson, Soft micro- and nanorobotics. *Annu. Rev. Control Robot. Auton. Syst.* **1**, 53–75 (2018).
19. S. Palagi, P. Fischer, Bioinspired microrobots. *Nat. Rev. Mater.* **3**, 113–124 (2018).
20. S.-J. Jeon, A. W. Hauser, R. C. Hayward, Shape-morphing materials from stimuli-responsive hydrogel hybrids. *Acc. Chem. Res.* **50**, 161–169 (2017).
21. A. Sidorenko, T. Krupenkin, A. Taylor, P. Fratzl, J. Aizenberg, Reversible switching of hydrogel-actuated nanostructures into complex micropatterns. *Science* **315**, 487–490 (2007).
22. J.-H. Na, A. A. Evans, J. Bae, M. C. Chiappelli, C. D. Santangelo, R. J. Lang, T. C. Hull, R. C. Hayward, Programming reversibly self-folding origami with micropatterned photocrosslinkable polymer trilayers. *Adv. Mater.* **27**, 79–85 (2015).
23. J. Cui, T.-Y. Huang, Z. Luo, P. Testa, H. Gu, X.-Z. Chen, B. J. Nelson, L. J. Heyderman, Nanomagnetic encoding of shape-morphing micromachines. *Nature* **575**, 164–168 (2019).
24. F. Li, D. P. Josephson, A. Stein, Colloidal assembly: The road from particles to colloidal molecules and crystals. *Angew. Chem. Int. Ed.* **50**, 360–388 (2011).
25. N. Vogel, M. Retsch, C.-A. Fustin, A. del Campo, U. Jonas, Advances in colloidal assembly: The design of structure and hierarchy in Two and Three dimensions. *Chem. Rev.* **115**, 6265–6311 (2015).
26. Z. Li, Q. Fan, Y. Yin, Colloidal self-assembly approaches to smart nanostructured materials. *Chem. Rev.* **122**, 4976–5067 (2022).
27. J. Henzie, M. Grünwald, A. Widmer-Cooper, P. L. Geissler, P. Yang, Self-assembly of uniform polyhedral silver nanocrystals into densest packings and exotic superlattices. *Nat. Mater.* **11**, 131–137 (2012).
28. T. Hueckel, G. M. Hocky, J. Palacci, S. Sacanna, Ionic solids from common colloids. *Nature* **580**, 487–490 (2020).
29. M. He, J. P. Gales, É. Ducrot, Z. Gong, G.-R. Yi, S. Sacanna, D. J. Pine, Colloidal diamond. *Nature* **585**, 524–529 (2020).
30. C. Avci, I. Imaz, A. Carné-Sánchez, J. A. Pariente, N. Tasios, J. Pérez-Carvajal, M. I. Alonso, A. Blanco, M. Dijkstra, C. López, D. Maspoch, Self-assembly of polyhedral metal–Organic framework particles into three-dimensional ordered superstructures. *Nat. Chem.* **10**, 78–84 (2018).
31. D. Lyu, W. Xu, J. E. L. Payong, T. Zhang, Y. Wang, Low-Dimensional Assemblies of metal-organic framework particles and mutually coordinated anisotropy. *Nat. Commun.* **13**, 3980 (2022).
32. K. Han, C. W. Shields IV, N. M. Diwakar, B. Bharti, G. P. López, O. D. Velev, Sequence-encoded colloidal origami and microbot assemblies from patchy magnetic cubes. *Sci. Adv.* **3**, e1701108 (2017).
33. T. Yang, B. Sprinkle, Y. Guo, J. Qian, D. Hua, A. Donev, D. W. M. Marr, N. Wu, Reconfigurable microbots folded from simple colloidal chains. *Proc. Natl. Acad. Sci. U.S.A.* **117**, 18186–18193 (2020).
34. C. van der Wel, R. K. Bhan, R. W. Verweij, H. C. Frijters, Z. Gong, A. D. Hollingsworth, S. Sacanna, D. J. Kraft, Preparation of colloidal organosilica spheres through spontaneous emulsification. *Langmuir* **33**, 8174–8180 (2017).
35. T. Loiseau, L. Lecroq, C. Volkringer, J. Marrot, G. Férey, M. Haouas, F. Taulelle, S. Bourrelly, P. L. Llewellyn, M. Latroche, MIL-96, a porous aluminum trimesate 3D structure constructed from a hexagonal network of 18-membered rings and μ3-oxo-centered trinuclear units. *J. Am. Chem. Soc.* **128**, 10223–10230 (2006).
36. M. Sindoro, A.-Y. Jee, S. Granick, Shape-selected colloidal mof crystals for aqueous use. *Chem. Commun.* **49**, 9576–9578 (2013).
37. D. Lyu, W. Xu, Y. Wang, Low-symmetry MOF-based patchy colloids and their precise linking via site-selective liquid bridging to form supra-colloidal and supra-framework architectures. *Angew. Chem. Int. Ed. Engl.* **134**, e202115076 (2022).
38. F. Gittes, B. Mickey, J. Nettleton, J. Howard, Flexural rigidity of microtubules and actin filaments measured from thermal fluctuations in shape. *J. Cell Biol.* **120**, 923–934 (1993).
39. Y. Mu, L. Lei, J. Zheng, W. Duan, Z. Wang, J. Tang, Y. Gao, Y. Wang, Binary phases and crystals assembled from active and passive colloids. *ACS Nano* **16**, 6801–6812 (2022).
40. R. Parreira, E. Özelçi, M. S. Sakar, Remotely controlled colloidal assembly of soft microrobotic artificial muscle. *Adv. Intell. Syst.* **2**, 2000062 (2020).
41. X. Hu, I. C. Yasa, Z. Ren, S. R. Goudu, H. Ceylan, W. Hu, M. Sitti, Magnetic soft micromachines made of linked microactuator networks. *Sci. Adv.* **7**, eabe8436 (2021).
42. M. Liu, L. Jin, S. Yang, Y. Wang, C. B. Murray, S. Yang, Shape morphing directed by spatially encoded, dually responsive liquid crystalline elastomer micro-actuators. *Adv. Mater.* **35**, 2208613 (2023).
43. H. Furukawa, K. E. Cordova, M. O'Keeffe, O. M. Yaghi, The Chemistry and applications of metal-organic frameworks. *Science* **341**, 1230444 (2013).
44. G. Lu, S. Li, Z. Guo, O. K. Farha, B. G. Hauser, X. Qi, Y. Wang, X. Wang, S. Han, X. Liu, J. S. DuChene, H. Zhang, Q. Zhang, X. Chen, J. Ma, S. C. J. Loo, W. D. Wei, Y. Yang, J. T. Hupp, F. Huo, Imparting functionality to a metal–organic framework material by controlled nanoparticle encapsulation. *Nat. Chem.* **4**, 310–316 (2012).
45. T. Hueckel, G. M. Hocky, S. Sacanna, Total synthesis of colloidal matter. *Nat. Rev. Mater.* **6**, 1053–1069 (2021).
46. Y. Li, F. Mou, C. Chen, M. You, Y. Yin, L. Xu, J. Guan, Light-controlled bubble propulsion of amorphous TiO_2/Au Janus micromotors. *RSC Adv.* **6**, 10697–10703 (2016).
47. G. Pérez-Sánchez, F. A. Vicente, N. Schaeffer, I. S. Cardoso, S. P. M. Ventura, M. Jorge, J. A. P. Coutinho, Rationalizing the phase behavior of triblock copolymers through experiments and molecular simulations. *J. Phys. Chem. C* **123**, 21224–21236 (2019).
48. K. Mortensen, J. S. Pedersen, Structural study on the micelle formation of poly(ethylene oxide)-poly(propylene oxide)-poly(ethylene oxide) triblock copolymer in aqueous solution. *Macromolecules* **26**, 805–812 (1993).
49. A. R. Khokhlov, A. Y. Grosberg, V. S. Pande, "Ideal polymer chain" in *Statistical Physics of Macromolecules* (AIP, 1994), pp. 1–78.
50. M. Rubinstein, R. H. Colby, "Ideal chains" in *Polymer Physics* (Oxford Univ. Press, 2003), pp. 49–96.

Acknowledgments: We thank Q. Zhang, P. Hua, and Y. Han (Hong Kong University of Science and Technology) for helping with the heating stage setup. **Funding:** Y.W. acknowledges the financial support from the General Research Fund, the Research Grants Council (RGC) of Hong Kong (project nos. 17314222 and 17307221); National Natural Science Foundation of China Excellent Young Scientists Fund 2020 (Hong Kong and Macau, project no. 22022206); and Innovation Award 2019 from the Croucher Foundation of Hong Kong. R.Z. acknowledges the financial support from Hong Kong Innovation and Technology Fund (grant nos. ITS/148/20 and ITS/178/20FP) and Croucher Foundation (CM/CT/CF/CIA/0688/19ay). **Author contributions:** D.L. and Y.W. conceived the project. D.L., W.X., W.D., and Y.M. synthesized the particles. D.L., W.X., and Z.W. conducted experiments and analyzed the data. N.Z. and R. Z. designed and set up the microscope. Y.W. supervised the project. D.L. and Y.W. wrote the manuscript. All other authors contributed to the revision. **Competing interests:** The authors declare that they have no competing interests. **Data and materials availability:** All data needed to evaluate the conclusions in the paper are present in the paper and/or the Supplementary Materials.

Submitted 18 February 2023
Accepted 30 May 2023
Published 30 June 2023
10.1126/sciadv.adh2250

ScienceAdvances

Biomimetic thermoresponsive superstructures by colloidal soft-and-hard co-assembly

Dengping Lyu, Wei Xu, Nansen Zhou, Wendi Duan, Zhisheng Wang, Yijiang Mu, Renjie Zhou, and Yufeng Wang

Sci. Adv. **9** (26), eadh2250. DOI: 10.1126/sciadv.adh2250